

J. MACROMOL. SCI.—PHYS., B41(3), 599–613 (2002)

1  
2  
3  
4  
5  
6  
7  
8  
9  
10  
11  
12  
13  
14  
15  
16  
17  
18  
19  
20  
21  
22  
23  
24  
25  
26  
27  
28  
29  
30  
31  
32  
33  
34  
35  
36  
37  
38  
39  
40  
41  
42  
43  
44

## CRYSTALLIZATION KINETICS OF COPOLY(ESTER IMIDE)S DERIVED FROM PBT, TRIMELLITIC ANHYDRIDE, AND ALIPHATIC DIAMINES

C. Wutz\* and S. Bartos

Institut für Technische und Makromolekulare Chemie, Universität  
Hamburg, Bundesstr. 45, D-20146, Hamburg, Germany

### ABSTRACT

The crystallization kinetics of copoly(ester imide)s based on poly(butylene terephthalate) (PBT), trimellitic anhydride, and diaminobutane (PEI-4), resp. diaminoethane (PEI-6) or diaminoethane (PEI-2) are investigated by means of time-resolved x-ray scattering employing synchrotron radiation. The PEI-4 and PEI-6 copolymers exhibit a remarkably high degree of crystallinity, which can be attributed to the formation of mixed crystals in the co-PEI-4 and to blockiness in the case of co-PEI-6. Whereas the pure PEI-4 forms large negatively birefringent spherulites, the co-PEI-4 and the PEI-6 homo- and copolymers form much smaller superstructures like axialites or ellipsoids. In the co-PEI-4 and co-PEI-6, the rate of crystallization is slower compared to the homopolymers due to the incorporation of the respective comonomer unit. The PEI-4 forms a second crystal modification upon drawing and subsequent crystallization, probably with a monoclinic unit cell. The PEI-6 crystallizes faster than PEI-4 due to the improved flexibility of the longer diamine component. In contrast, the crystallization of PEI-2 and its copolymers takes several hours and the equimolar co-PEI-2 remains completely amorphous.

*Key Words:* Poly(ester imide)s; Crystallization kinetics

---

\*Corresponding author. E-mail: christoph.wutz@desy.de

## INTRODUCTION

In a broader study, 1,4-diaminobutane (DAB) was used as a component for polyimides (1,2), poly(amide imide)s (3), and poly(ester imide)s in order to explore applications of DAB originally manufactured on a large scale for polyamide 4.6. One way to incorporate DAB into the commercial polyester poly(butylene terephthalate) (PBT) is the synthesis of *N,N*-butane- $\alpha,\omega$ -diyl-bis(trimellitimide) (4-BTI), which is in turn copolycondensed with dimethylterephthalate (DMT) and 1,4-butanediol (BD) in different compositions yielding copoly(ester imide)s of the chemical structure co-PEI-4 (see Fig. 1). About 0–100% of the terephthalate units in PBT was replaced by 4-BTI (4).

Furthermore, analogous copoly(ester imide)s PEI-2 and PEI-6 were synthesized using diaminoethane and diaminohexane, respectively.

The thermal stability and melt viscosity of these polymers have been investigated recently (4). This paper reports the crystallization behavior, the knowledge of which is also essential for injection molding. The samples were investigated during isothermal treatment by time-resolved x-ray scattering employing synchrotron radiation.

## EXPERIMENTAL

### Materials

All homo- and copoly(ester imide)s were synthesized by Bernd Schmidt and Cor Koning, DSM Research, Netherlands (4). Starting from 1,4-diaminoalkanes and trimellitic acid,  $\alpha,\omega$ -diaminoalkanebis(trimellitimide) was synthesized and subsequently esterified with methanol. Thermal copolycondensation with dimethylterephthalate in mole ratios from 0 to 100% and BD yielded a series of random copoly(ester imide)s with relative viscosities between 1.64 and 2.08 corresponding to molecular weights of 14,000–22,000 g/mol relative to PBT (4). All samples were melt-pressed and quenched into ice-water in order to obtain amorphous films. Isothermal crystallization was performed either starting from the glassy state or cooling the melt.

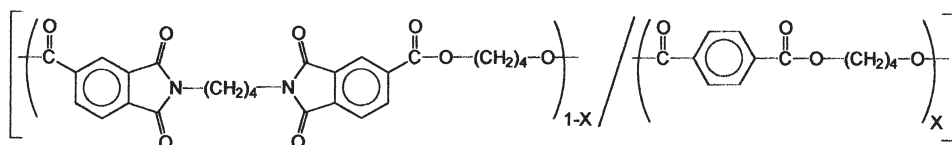


Figure 1. Chemical structure of co-PEI-4.

### Measurements

The differential scanning calorimetry (DSC) traces were recorded on a DuPont DSC in aluminum pans at a heating rate of  $10^{\circ}\text{C}/\text{min}$  ( $-10^{\circ}\text{C}/\text{hr}$  for cooling PEI-2). Wide-angle x-ray scattering (WAXS) was measured with a Siemens D500 diffractometer using Ni-filtered  $\text{Cu K}\alpha$ -radiation at  $\lambda = 0.154$  nm. The x-ray fiber pattern was obtained with a pin-hole camera on a flat film. The time-resolved WAXS measurements were performed employing synchrotron radiation with  $\lambda = 0.15$  nm at the polymer beamline (A2) of the Hamburger Synchrotron Laboratorium (HASYLAB) at the Deutsches Elektronensynchrotron (DESY) in Hamburg, Germany, which had been described in detail earlier (5). The WAXS was detected by a one-dimensional wire-counter with 30 sec acquisition time and normalized with respect to the primary beam intensity.

Molecular modeling calculations were performed on an SGI computer with the force field program InsightII/Discover (CFF91) by MicroSimulations at a torsion constrain of 1000 kcal/mol.

## RESULTS AND DISCUSSION

### Properties of Diaminobutane

The PEI-4 and all co-PEI-4 were melt-pressed, quenched in ice-water, and subjected to DSC measurements. Figure 2 depicts the DSC curve of PEI-4 [0/100] as an example. The glass transition step can be clearly detected at  $T_g = 77^{\circ}\text{C}$ . The broad crystallization exotherm is followed by the melting endotherm. The temperatures of the glass transition,  $T_g$ , the crystallization peak,  $T_c$ , and the melting,  $T_m$ , are listed in Table 1 for different PEI-4/PBT compositions (pure PBT

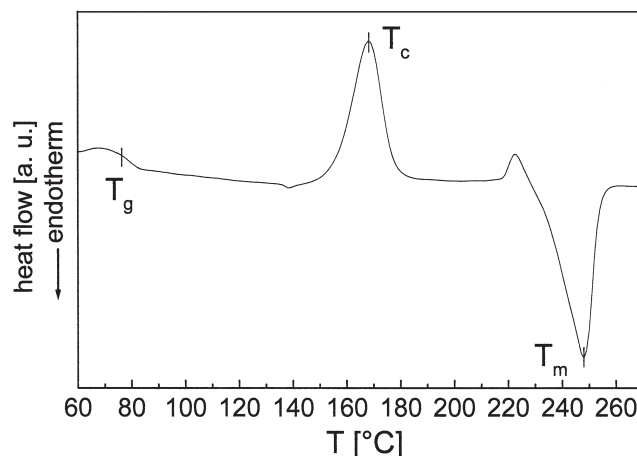


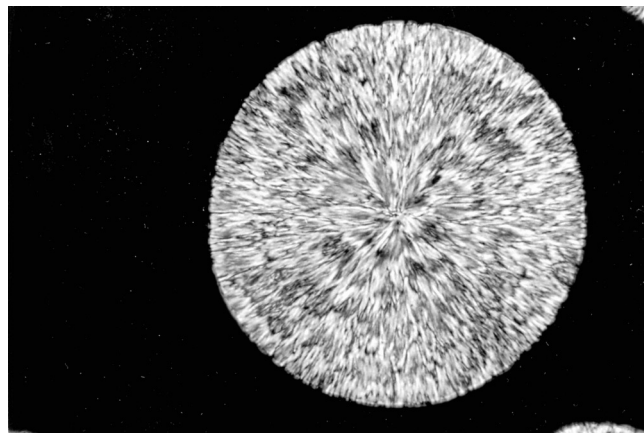
Figure 2. DSC heating curve of quenched PEI-4 [0/100] at a rate of  $10^{\circ}\text{C}/\text{min}$ .

133 **Table 1.** Temperatures of the Glass Transition  $T_g$ , Crystallization  $T_c$ , and Melting  $T_m$  from  
 134 Differential Scanning Calorimetry, Position of Wide-Angle X-Ray Scattering Reflections, and  
 135 Crystallinity of Different Co-Diaminobutanes

136 Composition	$T_g$ (°C)	$T_c$ (°C)	$T_m$ (°C)	$2\theta$ (°)	$x_c$ (%)
137 [100/0]	44	—	226	9.6, 12.9, 15.3, 19.4, 22.7, 23.6, 26.8	44
138 [90/10]	47	—	217	9.6, 13.0, 15.3, 19.4, 22.7, 23.6, 26.8	42
139 [80/20]	50	81	209	9.6, 13.1, 15.4, 19.4, 22.6, 23.6, 26.8	33
140 [70/30]	55	105	205	9.6, 13.2, 15.4, 19.4, 22.6, 23.4, 26.9	30
141 [60/40]	59	125	201	9.5, 13.3, 15.5, 19.3, —, 23.3, 27.0	28
142 [50/50]	66	142	203	9.3, 13.9, 15.6, —, —, 23, 1, 27.1	27
143 [40/60]	67	162	212	9.0, —, 15.8, —, —, 22.9, 27.1	29
144 [30/70]	81	167	220	9.0, 15.1, 16.1, —, —, 22.9, 26.4	28
145 [20/80]	92	188	231	9.0, 15.3, 16.5, —, —, 23.0, 25.7	32
146 [10/90]	94	170	239	9.0, 15.9, 17.1, 20.7, 23.1, 25.2, 29.2, 31.2	34
147 [0/100]	99	168	249	9.0, 16.1, 17.3, 20.6, 23.4, 25.2, 29.3, 31.4	40

149 was not amorphous). Differences between the values in the literature (4) might be  
 150 due to prior thermal treatment or different heating rates. The  $T_g$  increases  
 151 monotonously with the PEI content in agreement with the Fox equation (6).  
 152 The usual melting point depression by the co-condensation can be expressed by  
 153 Flory's equation (7). The melting temperatures go through a minimum at a  
 154 composition of [60/40]. The temperature of the maximum rate of crystallization  $T_c$   
 155 increases with higher BTI content in principle, but surprisingly the co-PEI-4  
 156 [80/20] crystallizes at a higher temperature than the pure PEI-4.

157 **F3** The microscopic extinction pattern between crossed polars in Fig. 3 shows  
 158 that the pure PEI-4 forms negatively birefringent, banded spherulites (8) of several  
 159 100  $\mu\text{m}$  in diameter. The spherulites formed by pure PBT are smaller and of  
 160



175 **Figure 3.** Microscopic extinction pattern between crossed polars of pure PEI-4 [0/100] after  
 176 50 min at 210°C.

## CRYSTALLIZATION KINETICS OF COPOLY(ESTER IMIDE)S

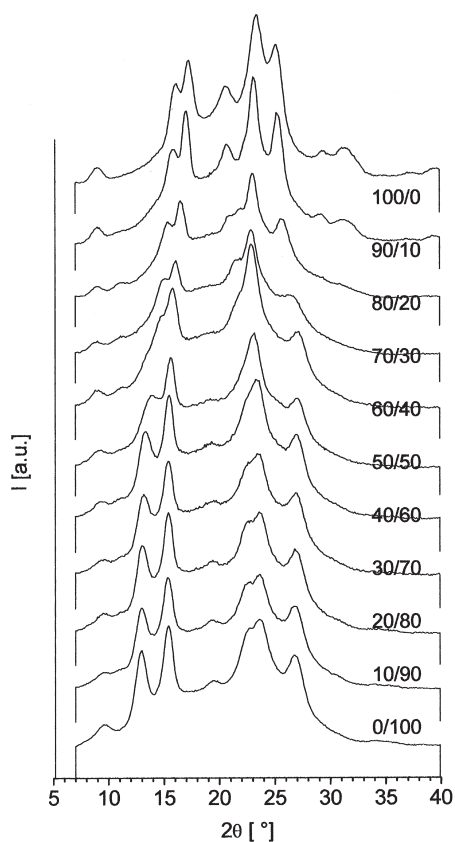
603

177 irregular shape and internal structure. The co-PEI-4 samples form much smaller  
178 superstructures like sheaves or ellipsoids.

179 For the crystallization of the co-PEI-4, the important question arises as to  
180 whether they form PBT crystals or PEI crystals and to what extent the  
181 copolymerization disturbs the crystallization. All samples were crystallized by  
182 annealing for 24 hr at a temperature of 20°C which is below the respective melting  
183 point. The WAXS curves of pure PBT [100/0], pure PEI-4 [0/100], and the various  
184 F4 co-PEI-4s in Fig. 4 reveal a substantial crystallinity for all samples and gradual  
185 changes in the peak positions with varying PEI-4 content.

186 After correction for background scattering, the amorphous halo was  
187 subtracted by drawing a smooth curve and the degree of crystallization  $x_c$  was  
188 calculated from the integral intensity of the crystal reflections divided by the entire  
189 scattering with an accuracy of  $\pm 2\%$ . The peak positions and the crystallinities are  
190 listed in Table 1.

191 With 40% the crystallinity in pure PEI-4 is slightly lower than in pure PBT  
192 (44%). As expected, the ability to form crystals is reduced by copolymerization.

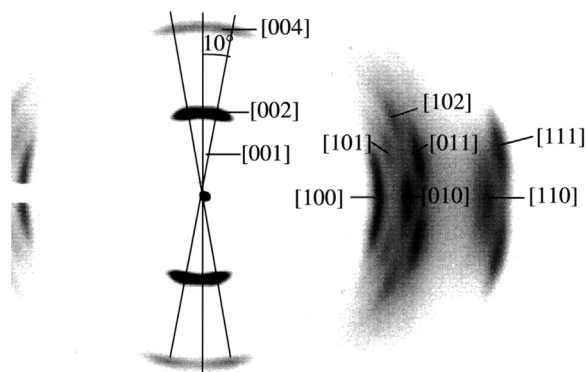


219 **Figure 4.** WAXS diffractograms of PBT [100/0], PEI-4 [0/100], and co-PEI-4 at various  
220 compositions.

221 Nevertheless, the co-PEI-4 still shows a surprisingly high degree of crystallization,  
 222 even at equimolar composition ( $x_c = 30\%$ ).

223 It might be argued that this crystallinity is a result of blockiness in the chain  
 224 sequence generated either in course of the polycondensation process or by  
 225 transesterification during the subsequent thermal treatment. In this case, the  
 226 WAXS diffractograms of the copolymers would display the reflections of both the  
 227 PBT and the PEI patterns. It turned out, however, that the measured WAXS curves  
 228 cannot be fitted by any combination of the homopolymer patterns. Therefore, we  
 229 assume that the crystal lattices of the homopolymers are distorted by the  
 230 incorporation of increasing amounts of the respective comonomer unit. By this,  
 231 the positions of the crystal reflections shift gradually and vanish eventually due to  
 232 changes in the form factor. Continuous changes in the WAXS patterns of  
 233 copolymers with variation of the composition have been observed frequently, but  
 234 examples of a complete analysis of the unit cell distortions are rare (9,10). The  
 235 WAXS patterns in Fig. 4 and the peak positions in Table 1 indicate that a PEI-4  
 236 crystal lattice is formed up to a PBT content up to 40%. For more than 70% PBT  
 237 content, the PBT sequences dominate the crystal lattice and the corresponding  
 238 WAXS reflections occur.

239 In the following, we try to find out whether the steady change in the WAXS  
 240 patterns of the copolymers can be caused by a similarity of the crystal structures of  
 241 PBT and PEI-4. For this purpose, PEI-4 was drawn into a fiber and crystallized  
 242 subsequently at 120°C for 24 hr with fixed ends. The x-ray fiber pattern acquired  
 243 F5 with a pin-hole camera is shown in Fig. 5. One observes a series of arc-shaped  
 244 reflections from which the crystal structure may be determined. Although the x-ray  
 245 pattern of the fiber, oriented perpendicular to the beam, does not display all crystal  
 246 reflections, it is striking that the radial positions of the detected reflections differ  
 247 completely from those in the powder pattern of the melt-crystallized sample (Fig. 4,  
 248 bottom; modification I). Obviously, the drawing and subsequent crystallization  
 249 result in a different crystal modification II. This different crystallization behavior  
 250 may be due to the following two reasons. First, the polymer has been quenched



264 **Figure 5.** X-ray fiber pattern of quenched PEI-4 crystallized subsequently at 120°C for 24 hr.

during fiber spinning and the subsequent crystallization from the glassy state may result in a modification which differs from the one formed upon cooling the melt. Second, the change in the crystal structure may be due to the molecular orientation. In order to distinguish between these two influences, a PEI-4 sample was melt-pressed, quenched into the glassy state, and annealed subsequently in the same manner as the fiber. The WAXS pattern of this sample matches exactly the one of the melt-crystallized PEI-4, indicating that the formation of modification II is clearly a result of the molecular orientation. The DSC heating curve of the crystallized PEI-4 fiber reveals that the melting point of modification II is essentially the same as the  $T_m$  of modification I (see Table 1).

From the position and intensities of the reflections in the fiber pattern (Fig. 5), the unit cell of the PEI-4 modification II can be calculated. A series of reflections close to the meridian is particularly conspicuous, one of which at  $2\theta = 7.5^\circ$  has the highest intensity. These meridional reflections result from differences in the electron densities along the molecular chain and resemble the layer reflections of smectic-crystalline fibers. However, these spots represent the first, second, and fourth order of the reflection at  $2\theta = 3.75^\circ$ , corresponding to an interplanar spacing of 2.4 nm. The fact that the second-order reflection has a much higher intensity than the first order is due to the large difference in the electron densities between the aromatic and aliphatic units. Their regular sequence represents a sublattice with a spacing of 1.2 nm. Due to head-to-head and tail-to-tail linkages of the asymmetrical imide groups, a superlattice is generated with a spacing of 2.4 nm in good agreement with the monomer length of 2.3 nm calculated by computer modeling for an isolated molecule.

As can be seen from the second and fourth order, the [001]-reflections exhibit an inclination of  $\varphi = 10^\circ$  with respect to the meridian. Assuming the  $c$ -axis of the unit cell to be oriented parallel to the fiber direction, the azimuthal angle  $\varphi$  corresponds to the tilt angle  $\beta$  of the  $a, b$ -plane. We conclude that the crystal lattice is not orthogonal, but either monoclinic or triclinic. The limited number of reflections and their different intensities suggest a monoclinic unit cell. In the equatorial direction one can recognize a series of reflections, three of which are located on the equator  $[hk0]$ , three pairs occur on the first layer line  $[hk1]$ , and one pair on the second layer line  $[hk2]$ . Although the limited number of reflections in the fiber diagram does not provide an appropriate means for a clear-cut analysis of the crystal structure, the attempt was made to index the reflections assuming a monoclinic unit cell with the parameters  $a = 0.56$  nm,  $b = 0.47$  nm,  $c = 0.235$  nm, and  $\beta = 100^\circ$  by Eq. (1) (11).

$$d = \left[ \frac{(h^2/a^2) + (l^2/c^2) - (2hl/ac)\cos\beta}{\sin^2\beta} + \frac{k^2}{b^2} \right]^{-1/2} \quad (1)$$

**T2** The measured and calculated scattering angles listed in Table 2 are in good agreement.

309 **Table 2.** Comparison of Experimental and Calculated Scattering Data Assuming a Monoclinic  
 310 Unit Cell with  $a = 0.56$  nm,  $b = 0.47$  nm,  $c = 2.35$  nm, and  $\beta = 100^\circ$

311	$[h,k,l]$	$2\theta$ ( $^\circ$ ), Experimental Values <sup>a</sup>	$2\theta$ ( $^\circ$ ), Calculated Values	$d$ (nm), Calculated Values
312	[1,0,0]	16.0	16.1	0.55
313	[0,1,0]	18.5	18.9	0.47
314	[1,1,0]	24.8	24.9	0.36
315	[1,0,1]	17.4	17.1	0.52
316	[0,1,1]	19.6	19.2	0.46
317	[1,1,1]	25.9	25.6	0.35
318	[1,0,2]	18.7	19.0	0.47
319	[0,0,1]	3.8	3.8	2.35
320	[0,0,2]	7.5	7.6	1.18
320	[0,0,4]	15.0	15.3	0.60

321 <sup>a</sup>Error limit  $\pm 0.4^\circ$ .

322  
 323  
 324  
 325 Since the strong meridional reflections in the fiber pattern of PEI-4 resembles  
 326 a higher ordered smectic-crystalline  $S_H$ -phase (12), another x-ray pattern was  
 327 **Q1** taken from the drawn fiber before crystallization. Although no LC-phases have  
 328 been detected during cooling of unoriented PEI-4 samples, rapid drawing from the  
 329 melt and quenching could freeze a smectic mesophase in principle. However, the  
 330 x-ray pattern of the PEI-4 fiber, prior to thermal treatment, displays no layer  
 331 reflection so that the formation of a smectic LC-phase can be excluded.  
 332 Unfortunately, no oriented samples of modification I could be obtained so that a  
 333 comparison to the PBT crystal structure was not possible.

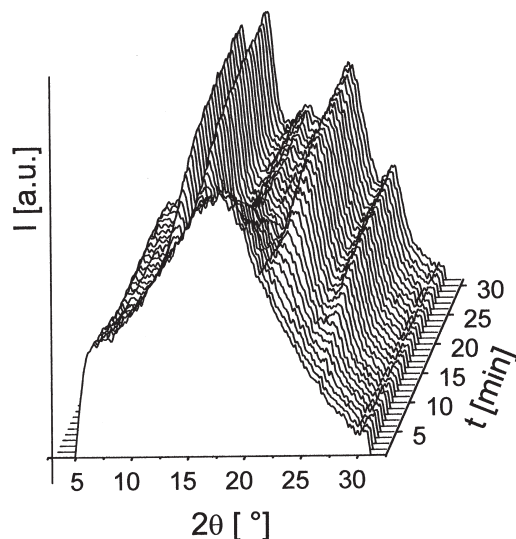


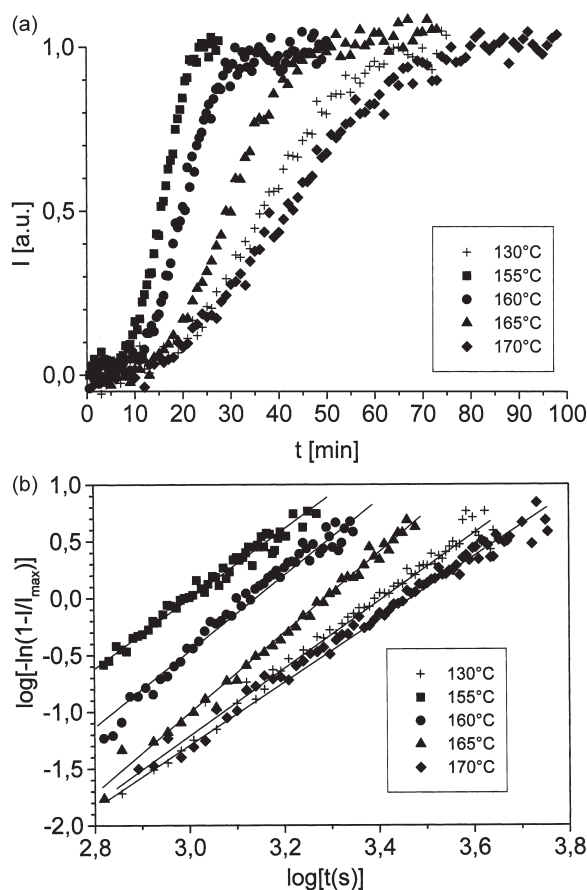
**Figure 6.** Change of WAXS during isothermal crystallization of PEI-4 [0/100] at  $190^\circ\text{C}$ .



## CRYSTALLIZATION KINETICS OF COPOLY(ESTER IMIDE)S

607

353 The pure PEI-4 and the co-PEI-4 were crystallized isothermally in order to  
 354 study the influence of the composition on the crystallization kinetics by means of  
 355 F6 time-resolved WAXS. Figure 6 shows the change of the WAXS pattern during  
 356 crystallization of PEI-4 [0/100] at 190°C as an example. The crystal reflections  
 357 grow at the expense of the amorphous halo. For the investigation of the  
 358 crystallization kinetics, it is not necessary to evaluate the absolute degree of  
 359 crystallinity; the increase in integral intensity of the WAXS reflections is  
 360 sufficient. Since the isotropic melt of PEI-4 and co-PEI-4 can be frozen into the  
 361 glassy state by quenching below  $T_g$ , it is reasonable to investigate the  
 362 crystallization kinetics at high temperatures starting from the melt and at low  
 363 F7 temperatures starting from the glassy state. As an example, Fig. 7a shows the  
 364 integral intensity  $I$  of the WAXS reflections as a function of time for co-PEI-4  
 365 [40/60] at different temperatures. The curves exhibit the typical sigmoidal shape  
 366 and the evaluation of the kinetics according to Avrami's law (13–15) results in



395 **Figure 7.** (a) Integral WAXS reflection intensity  $I$  as a function of time during crystallization of  
 396 co-PEI-4 [40/60] at different temperatures and (b) Avrami plot.

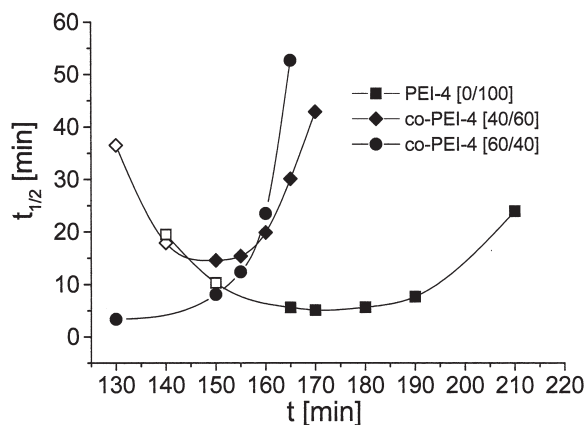
397 exponent  $n$  between 2.5 and 3.3 (see Fig. 7b) in agreement with the observed  
 398 **F8** growth of three-dimensional superstructures. In Fig. 8, the half time of the  
 399 crystallization is plotted as a function of the crystallization temperature. Open  
 400 symbols indicate crystallization from the glassy state; full symbols represent  
 401 crystallization from the melt. The fastest crystallization with a half time of 5 min  
 402 occurs in the temperature range between 160 and 180°C in agreement with the  $T_c$   
 403 measured by DSC. The crystallization is slower at lower temperatures due to  
 404 reduced molecular mobility and at higher temperatures due to a lower nucleation  
 405 rate.

406 Essentially the same behavior is found for all samples, but the maximum  
 407 rates of crystallization and the corresponding temperatures change with  
 408 composition. For co-PEI-4 [40/60], the fastest crystallization occurs between  
 409 140 and 155°C, approximately 15°C lower than in pure PEI-4, and the shortest half  
 410 time is 13 min, which is 8 min more than for pure PEI-4. The incorporation of  
 411 flexible PBT units improves the mobility of the molecules at lower temperatures,  
 412 but hinders the formation of the PEI-4 crystals.

413 **T3** This hindrance becomes more obvious in Table 3 where the half times of  
 414 crystallization at  $T_c = 160$  and 170°C are compared for different co-PEI-4  
 415 compositions. The crystallization of the co-PEI-4 becomes slower with increasing  
 416 fraction of PBT up to the equimolar composition. At higher PBT contents, the  
 417 formation of PBT crystals becomes faster again.

### 419 Properties of Diaminohexane

420 The crystallization of PEI-6 based on trimellitic acid, diaminohexane, and  
 421 butanediol was investigated in order to study the influence of the prolongation of  
 422  
 423  
 424



438  
 439 **Figure 8.** Half time of crystallization of PEI-4 [0/100], co-PEI-4 [40/60], and co-PEI-4 [60/40] as a  
 440 function of crystallization temperature. Full symbols indicate crystallization from the melt, open  
 symbols from the glassy state.

## CRYSTALLIZATION KINETICS OF COPOLY(ESTER IMIDE)S

609

**Table 3.** Temperatures of Glass Transition  $T_g$  and Melting  $T_m$  from Differential Scanning Calorimetry Measurements, Position of Wide-Angle X-Ray Scattering Reflections, and Degree of Crystallization of Different Co-Diaminoethanes

Composition	$T_g$ (°C)	$T_m$ (°C)	$2\theta$ (°)	$x_c$ (%)
[100/0]	44	226	9.6, 12.9, 15.3, 19.4, 22.7, 23.6, 26.8	44
[80/20]	62	200	9.1, 15.8, 17.1, 20.8, 23.2, 25.2	28
[60/40]	89	— <sup>a</sup>	— <sup>a</sup>	— <sup>a</sup>
[30/70]	113	216	19.3, 21.5	8
[10/90]	124	228	8.7, 11.2, 18.2, 28.6	43
[0/100]	133	234	8.7, 11.2, 18.2, 22.5, 26.0, 28.5	47

<sup>a</sup>Very low crystallinity.

the diamine unit compared to PEI-4 on the thermal behavior of the polymer. Additionally, in various co-PEI-6s the influence of the composition on the formation of the crystal lattice was studied by means of WAXS. Figure 9 shows the WAXS diffractograms of the crystallized pure PBT [100/0], pure PEI-6 [0/100], and different co-PEI-6s. The crystal reflections of PEI-6 occur at  $2\theta =$

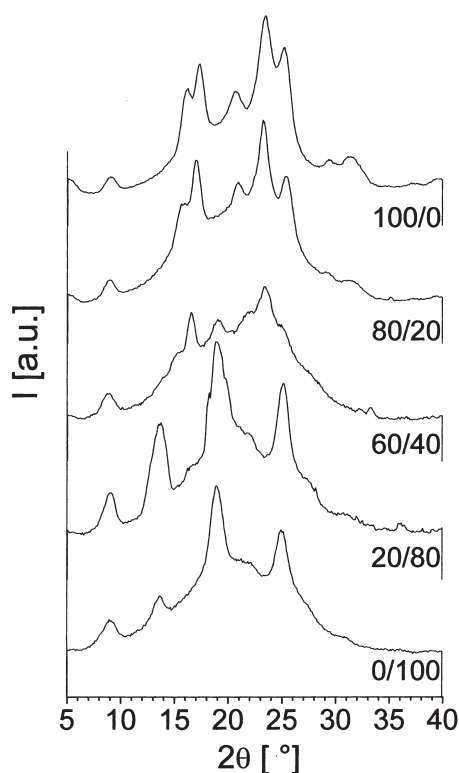


**Figure 9.** WAXS diffractograms of PBT [100/0], PEI-6 [0/100], and co-PEI-6 at various compositions.

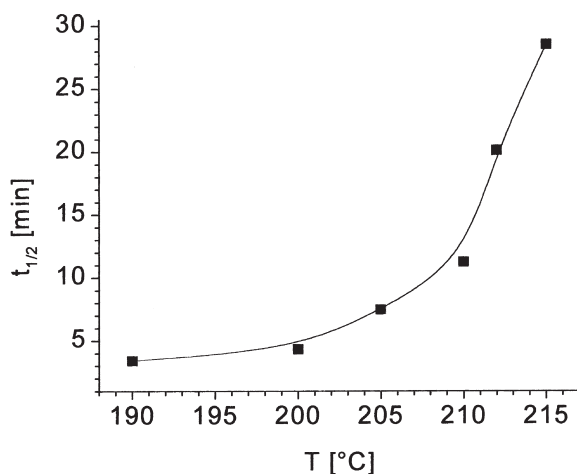
485 9.1, 13.6, 18.8, and 25.0°. The observation that all peak positions differ from those  
486 of PEI-4 indicates that the prolongation of the diaminoalkane component changes  
487 not only the *c*-axis of the unit cell but also the entire crystal structure. The  
488 comparison with the WAXS patterns of PEI-2 (see below) reveals that shortening  
489 causes the same effect.

490 The co-PEI-6 [80/20] crystallizes to form a slightly distorted PBT lattice,  
491 while the co-PEI-6 [20/80] forms PEI-6 crystals. The co-PEI-6 [60/40] has a  
492 crystallinity of 18% from both PBT- and PEI-6 crystals, which gives rise to weak  
493 WAXS reflections originating partly from a distorted PBT lattice ( $2\theta = 16.6$  and  
494  $23.5^\circ$ ) and partly from the PEI-6 lattice ( $2\theta = 18.9^\circ$ ). In contrast to PEI-4, this  
495 coexistence of both crystal modifications clearly indicates a blocky character of  
496 the comonomer sequence in the co-PEI-6 molecular chains.

497 The pure PEI-6 was crystallized isothermally at different temperatures. The  
498 half times of crystallization plotted as a function of crystallization temperature in  
499 **F10** Fig. 10 reveal that the rate of crystallization becomes slower with increasing  
500 temperature above 200°C. Below 200°C, the half time is shorter than 4 min, and  
501 thus, the kinetics of the process cannot be determined precisely by the used set-up.  
502 In comparison with PEI-4 (Fig. 8), PEI-6 crystallizes faster at identical  
503 temperatures (190 and 210°C). This observation can be explained by the improved  
504 flexibility and mobility of the chain segments due to the substitution of the butane  
505 unit between the aromatic segments with a longer hexane unit.

### 507 Properties of Diaminoethane

508 It turned out that the crystallization of PEI-2 (based on diaminoethane) and  
509 its copolymers takes an extremely slow course, so that it is not easy to obtain  
510  
511

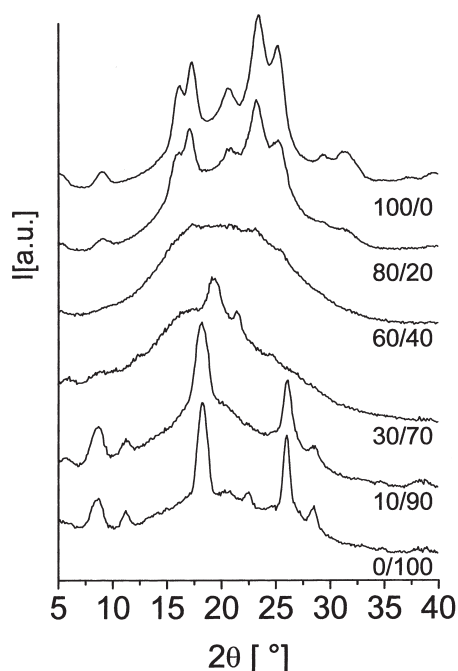


512  
513  
514  
515  
516  
517  
518  
519  
520  
521  
522  
523  
524  
525  
526  
527 **Figure 10.** Half time of crystallization of PEI-6 [0/100] as a function of crystallization  
528 temperature.

## CRYSTALLIZATION KINETICS OF COPOLY(ESTER IMIDE)S

611

529 crystalline samples at all. Even cooling at a rate of  $-10^{\circ}\text{C/hr}$  did not give rise to an  
530 exothermal crystallization peak in the DSC curve. However, annealing at  $200^{\circ}\text{C}$   
531 for 48 hr yielded crystalline PEI-2 and co-PEI-2, which were subjected to DSC  
532 heating experiments at a rate of  $10^{\circ}\text{C/min}$  and WAXS. The glass transition and  
533 melting temperatures, the position of the WAXS reflections, and the degree of  
534 crystallization of the PEI-2 and its copolymers are listed in Table 3.  $T_g$  is elevated  
535 by increasing the fraction of the imide component, as observed previously for PEI-  
536 4. Once again, the melting temperature passes through a minimum. For the co-  
537 PEI-2 [60/40], no melting point could be evaluated because the crystallinity is very  
538 F11 low as evidenced by the virtually amorphous WAXS pattern shown in Fig. 11. In  
539 the case of PEI-2, the obstruction effect of the copolymerization upon the  
540 crystallization is obvious. Possibly, this observation indicates a more random  
541 sequence of the comonomer units as compared to co-PEI-6. The co-PEI-2 [80/20]  
542 forms a slightly disturbed PBT lattice with 37% crystallinity. The co-PEI-2  
543 [30/70] exhibits two weak WAXS reflections at  $2\theta = 19.3$  and  $21.5^{\circ}$  which can be  
544 attributed neither to PBT crystals nor to the crystal lattice formed by the pure PEI-  
545 2. Whether the occurrence of these reflections is due to an extreme case of lattice  
546 distortion or the formation of a mixed crystal cannot be deduced in a  
547 straightforward manner. A PBT content of 10% does not affect the formation of  
548 PEI-2 crystals significantly.



571 **Figure 11.** WAXS of PBT [100/0], PEI-2 [0/100], and co-PEI-2 with different compositions (peak  
572 positions listed in Table 3).

573 The crystallization of PEI-2 and its copolymers is so slow that it would need  
574 too much measuring time at the synchrotron source to study its kinetics. On the  
575 other hand, the question arises how the small change in the chemical structure  
576 compared to PEI-4 affects the crystallization behavior so drastically. It might be  
577 presumed that conformational changes in the short diamino-component, necessary  
578 for crystallization, are hampered by the proximity of the voluminous carbonyl  
579 groups. Therefore, the energy of an isolated PEI-2 chain segment, as a function of  
580 the C–C bond angle, has been determined by molecular modeling using force field  
581 calculations. As expected, the trans-conformation has the lowest energy. The  
582 overall rotational energy barrier amounts to 5 kcal/mol ( $\cong$  20 kJ/mol). This value  
583 is only slightly larger than the theoretical potential barrier height encountered in  
584 rotational isomerization about unsubstituted C–C bonds (16), and it is low  
585 compared to the activation energies measured for crystallization of conventional  
586 polymers [e.g., PET,  $E_a = 20\text{--}60$  kcal/mol (17–19)]. As a result, the interactions  
587 between adjacent imide groups cannot serve as an explanation for the slow  
588 crystallization kinetics of PEI-2. Moreover, a relationship between flexibility of  
589 the molecular chain and crystallization rate is evidenced, which is observed in the  
590 comparison of the crystallization behavior of the polyesters PET and PBT as well.

## 593 CONCLUSION

594  
595 For all three poly(ester imide)s, PEI-2, PEI-4, and PEI-6, copolymerization  
596 with PBT results in a melting point depression. Nevertheless, the PEI-4 and PEI-6  
597 copolymers with PBT exhibit a relatively high degree of crystallinity. An  
598 incorporation of 30% PBT into the PEI-4 changes the WAXS pattern only slightly.  
599 Even the equimolar copolymers give rise to strong crystal reflection. In contrast to  
600 the PEI-6 and PEI-4, the short diamino-component in PEI-2 reduces the flexibility  
601 of the chain in a way that the crystallization rate is decreased greatly.

## 604 ACKNOWLEDGMENTS

605  
606 The authors thank C. Koning and DSM Research, Netherlands, for providing the  
607 poly(ester imide) samples synthesized by Dr. B. Schmidt. We also acknowledge the  
608 molecular modeling calculations performed by M. Arndt-Rosenau.

## 610 REFERENCES

- 611  
612 Q2 1. Koning, C.E.; Teuwen, L.; Meijer, E.W.; Moonen, J. *Polymer* **1994**, *35*, 4889.  
613 Q2 2. Koning, C.E.; Teuwen, L.; Bulters, M. *Polym. Eng. Sci.* **1996**, *36*, 1347.  
614 Q3 3. Koning, C.E., submitted for publication.  
615 4. Schmidt, B.; Koning, C.E.; Buning, G.H.W.; Kricheldorf, H.R. *J. Macromol. Sci.—*  
616 *Pure Appl. Chem.* **1997**, *A34* (5), 759–774.

## CRYSTALLIZATION KINETICS OF COPOLY(ESTER IMIDE)S

613

Q4

- 617 Q2 5. Elsner, G.; Zachmann, H.G.; Milch, J.R. *Makromol. Chem.* **1981**, *182*, 657.
- 618 Q2 6. Fox, T.G. *Bull. Am. Phys. Soc.* **1956**, *1*, 123.
- 619 Q2 7. Flory, P.J. *J. Chem. Phys.* **1949**, *17*, 223.
- 620 Q2 8. Keller, A. *J. Polym. Sci.* **1955**, *17*, 291.
- 621 Q2 9. Redding, F.P.; Walter, E.R. *J. Polym. Sci.* **1959**, *37*, 555.
- 622 Q2 10. Chatani, Y.; Takizawa, T.; Murahashi, S. *J. Polym. Sci.* **1962**, *62*, S27.
- 623 11. Alexander, L.E. *X-Ray Diffraction Methods in Polymer Science*; Wiley: New York, 1969; 542.
- 624 Q5
- 625 Q2 12. Wutz, C.; Gieseler, D.; Maevis, T.; Stribeck, N. *Macromolecules* **1999**, *32*, 4658.
- 626 Q2 13. Avrami, M. *J. Chem. Phys.* **1939**, *7*, 1103.
- 627 Q2 14. Avrami, M. *J. Chem. Phys.* **1940**, *8*, 212.
- 628 Q2 15. Avrami, M. *J. Chem. Phys.* **1941**, *9*, 177.
- 629 16. Flory, P.J. *Statistical Mechanics of Chain Molecules*; Interscience: New York, 1969.
- 630 Q2 17. Cobbs, W.H.; Burton, R.L. *J. Polym. Sci.* **1953**, *10*, 275.
- 631 Q2 18. Miller, B. *J. Appl. Polym. Sci.* **1967**, *11*, 2343.
- 632 19. Mayhan, K.G.; James, W.J.; Bosch, W.J. *J. Appl. Polym. Sci.* **1965**, *9*, 3605.

Q2

Received July 13, 2000

Revised August 22, 2000

Accepted September 15, 2000

633  
634  
635  
636  
637  
638  
639  
640  
641  
642  
643  
644  
645  
646  
647  
648  
649  
650  
651  
652  
653  
654  
655  
656  
657  
658  
659  
660